ACCSCIENCE PUBLISHING

International Journal of Bioprinting

RESEARCH ARTICLE

Near-infrared controlled release of mesenchymal stem cells secretome from bioprinted graphene-based microbeads for nerve regeneration

Giordano Perini[1,2], Valentina Palmieri[2,3], Marcello D'Ascenzo[1,2], Claudia Colussi[2,4], Claudio Grassi[1,2], Ginevra Friggeri[2], Alberto Augello[2], Lishan Cui[1], Massimiliano Papi[1,2]*, and Marco De Spirito[1,2]

[1]Dipartimento di Neuroscienze, Università Cattolica del Sacro Cuore, Largo Francesco Vito 1, 00168 Rome, Italy

[2]Fondazione Policlinico Universitario A. Gemelli IRCSS, 00168 Rome, Italy

[3]Istituto dei Sistemi Complessi, CNR, Via dei Taurini 19, 00185 Rome, Italy

[4]Istituto di analisi dei sistemi ed informatica "Antonio Ruberti," CNR, Via dei Taurini 19, 00185 Rome, Italy

(This article belongs to the *Special Issue: Advances in 3D bioprinting for regenerative medicine and drug screening*)

Abstract

Nerve damage is a prevalent and debilitating condition with limited treatment options. Recent years have seen an increased incidence of neural damage due to factors such as aging populations and traumatic brain injuries. Addressing the urgent need for effective therapies, this study explores the controlled delivery of mesenchymal stem cells (MSCs) secretome, a complex mixture of bioactive factors, which is currently being investigated for its potential in nerve regeneration. The secretome offers significant advantages over stem cells themselves, as it can be more easily characterized and controlled, enabling precise regulation of therapeutic interventions. However, the challenge lies in delivering the secretome specifically to the target anatomical region. To overcome this limitation, we propose a novel approach utilizing near-infrared (NIR) radiation-responsive bioprinted alginate-graphene oxide (AGO) microbeads. Graphene oxide (GO) is a highly biocompatible material with unique properties, including NIR responsiveness, enabling controlled release of therapeutic agents upon NIR exposure. We hypothesized that AGO microbeads could encapsulate MSCs secretome and release it in a controlled manner using NIR radiation. To investigate our hypothesis, controlled damage was induced to hippocampal neurons, and MSCs secretome was encapsulated within AGO microbeads. Subsequently, NIR radiation was applied to trigger the release of the secretome. We compared the efficacy of MSCs secretome with that of astrocytes, which also possess nerve growth and proliferation-promoting capabilities. Our findings demonstrated that the controlled release of MSCs secretome from AGO microbeads through non-invasive NIR radiation significantly promoted the proliferation and regeneration of neurons following nerve injury. AGO microbeads offer multiple advantages over conventional delivery methods, including precise control over the timing, location, and dosage of therapeutic agents. Furthermore, the potential for reduced immunogenicity and tumorigenicity enhances the safety profile of the therapy. Consequently, this study presents a promising avenue for the development of MSC-based therapies for nerve regeneration, with implications for the treatment of various neuropathies and injuries.

***Corresponding author:**
Massimiliano Papi
(massimiliano.papi@unicatt.it)

Citation: Perini G, Palmieri V, D'Ascenzo M, *et al*., 2023, Near-infrared controlled release of mesenchymal stem cells secretome from bioprinted graphene-based microbeads for nerve regeneration. *Int J Bioprint*. https://doi.org/10.36922/ijb.1045

Received: June 5, 2023
Accepted: July 10, 2023
Published Online: August 4, 2023

Keywords: 3D Bioprinting; Near-Infrared Radiation; Graphene Oxide; Alginate Microbeads; Neural Regeneration

1. Introduction

Nerve damage is a major cause of disability worldwide, with limited treatment options available[1]. Neural damage refers to any injury or trauma to the cells, fibers, or pathways of the nervous system[2-4]. It can occur in the brain, spinal cord, or peripheral nerves, and can result from a variety of causes, including physical trauma, infection, toxicity, or degenerative diseases such as Alzheimer's or Parkinson's[4-9]. Neural damage can have severe and often irreversible consequences, including loss of function, memory, and cognition[10,11]. In recent years, the incidence of neural damage has increased due to factors such as aging populations and the rise in traumatic brain injuries[12,13]. As a result, there is a growing need for a better understanding of the mechanisms underlying neural damage and the development of new therapeutic strategies to mitigate its effects[14-16]. Symptoms of nerve damage can include numbness, tingling, pain, weakness, and loss of coordination, which can significantly impact an individual's quality of life[17-19]. Despite its prevalence, current treatments for neural damage are limited, and often involve management of symptoms rather than addressing the underlying causes[20-24].

Mesenchymal stem cells (MSCs) have shown promise in the treatment of neural damage due to their ability to differentiate into neuronal cells and modulate the immune response[25-28]. However, recent studies have suggested that the secretome of MSCs—the complex mixture of growth factors, cytokines, and extracellular vesicles they secrete—may play a key role in promoting neural regeneration[29,30]. The secretome has been shown to have immunomodulatory, anti-inflammatory, and neuroprotective effects, and can promote the survival, growth, and differentiation of neurons[31-33]. Notably, the secretome offers distinct advantages over stem cells themselves for stem therapies, as it can be characterized and controlled more easily, allowing for precise regulation and optimization of therapeutic interventions[34,35]. This enhanced suitability of the secretome holds the potential for more predictable and targeted outcomes in neural regeneration therapies. However, a critical challenge associated with the use of the secretome lies in its controlled administration to the specific anatomical district where it is needed[36,37]. Unlike the stem cells, which can be directly transplanted into the target area, the secretome requires careful delivery methods to ensure its localized and targeted action[38,39]. Strategies such as encapsulation within biomaterials or the use of specialized delivery systems are being explored to address this concern, which is crucial to harness the full potential of the secretome in neural regeneration therapies[40,41].

In this study, we propose a novel approach for the controlled delivery of MSCs secretome for nerve regeneration using near-infrared (NIR) radiation-responsive bioprinted alginate-graphene oxide (AGO) microbeads[42-44]. Graphene oxide (GO) is a highly biocompatible material that has shown to possess unique properties, including NIR responsiveness, which allows for the controlled release of therapeutic agents upon exposure to NIR radiation[45,46]. We hypothesized that AGO microbeads could be used to encapsulate and release in a controlled manner through NIR the secretome of MSCs. To test our hypothesis, we first induced controlled damage to hippocampal neurons. We then encapsulated MSCs secretome in AGO microbeads and exposed them to NIR radiation. We then compared the effectiveness of the secretome of MSCs with the secretome from astrocytes, which is also known to promote nerve growth and proliferation[47-52]. Our results demonstrated that the controlled release of MSCs secretome through non-invasive NIR from AGO microbeads promoted significant proliferation and regeneration of hippocampal neurons following nerve injury. The use of AGO microbeads offers several advantages over conventional delivery approaches, including the ability to control the timing, location, and dose of therapeutic agents, as well as the potential for reduced immunogenicity and tumorigenicity. Overall, our approach provides a promising new avenue for the development of MSC-based therapies for nerve regeneration, with implications for the treatment of various neuropathies and injuries.

2. Materials and methods

2.1. Cell culture

Primary cultures of hippocampal neurons were obtained from E15-18 C57BL/6 mice embryos as described previously and in accordance with the Ethics Committee of the Università Cattolica del Sacro Cuore and in compliance with Italian Ministry of Health guidelines, with national laws (Legislative Decree 116/1992), and European Union guidelines on animal research (No. 86/609/EEC) [53,54].

Briefly, the mouse cortex was dissected in cold CMF-HBSS (Ca^{2+} and Mg^{2+} free Hank's balanced salt solution containing 1 mM pyruvate, 15 mM 4-(2-hydroxyethyl)-1-piperazineethanesulfonic acid, HEPES, and 10 mM $NaHCO_3$). Tissues were then incubated for 10 min at 37°C in phosphate-buffered saline (PBS) containing trypsin-ethylenediaminetetraacetic acid (0.025%/0.01% w/v;

Biochrom), and the tissue was mechanically dissociated at room temperature with a fire-polished Pasteur pipette. The cell suspension was harvested and centrifuged at 235 × g for 8 min. The pellet was suspended in 88.8% Minimum Essential Medium (Biochrom), 5% fetal bovine serum (FBS), 5% horse serum, 1% glutamine (2 mM), 1% penicillin–streptomycin–neomycin antibiotic mixture (Invitrogen), and glucose (25 mM). Cells were plated at a density of 105 cells/mL on a 24-well plate precoated with poly-L-lysine (0.1 mg/mL; Sigma). Twenty-four hours later, the culture medium was replaced with a mixture of 96.5% neurobasal medium (Invitrogen), 2% B-27 (Invitrogen), 0.5% glutamine (2 mM), and 1% penicillin–streptomycin–neomycin antibiotic mixture. After 72 h, this medium was replaced with a glutamine-free version of the same medium, and the cells were grown for 10 more days before experiments. All cell lines were cultivated in T75 flasks and kept at 37°C in 5% CO_2 humidity. Mesenchymal stem cells were purchased from the American Type Culture Collection (ATCC). Cells were maintained in Dulbecco's modified Eagle's medium (Sigma-Aldrich) supplemented with 10% FBS (EuroClone), 2% penicillin–streptomycin (Sigma-Aldrich), and 2% L-glutamine (Sigma-Aldrich) on T25 flasks. After three passages, supernatant was gathered at 24 h from the change of culture medium and centrifuged at 1000 rpm for 10 min. Supernatant was then stored at -80°C for further use.

2.2. Bioprinting of alginate-graphene oxide microbeads

To bioprint AGO microbeads, a biocompatible bioink composed of the mixture of the two materials was first prepared. Alginate was kept at a concentration of 1.5% w/v, while GO was added at different final concentrations for further tests: 0.5, 0.2, and 0.1 mg/mL. Control microbeads were prepared without GO. Culture medium, astrocyte-conditioned medium (ACM; ScienCell), and MSCs secretome were added at a ratio 1:1 with respect to AGO. The mixture was then loaded into a bioprinting cartridge and transferred on an electromagnetic droplet printhead of BIO X bioprinter (Cellink, BICO Company). Bioprinting was performed at room temperature, extruding microbeads with a speed of 50 mm/s and a pressure of 120 kPa. An open time of 100 miliseconds (ms) and a cycle time of 1000 ms were applied to set the number of extruded beads. The droplets were extruded on a 6-well (Corning) filled with a 2% w/v $CaCl_2$ solution. The microbeads were left crosslinking for 10 min, and then they were carefully gathered and observed under the optical microscope of Cytation 3 Cell Imaging Multi-Mode Reader (Biotek).

2.3. Characterization of microbeads

Scanning electron microscopy (SEM) images were acquired to investigate the surface composition of the microbeads. Samples were dehydrated and sputter-coated with gold. They were then imaged with SEM Supra 25 (Zeiss). Images were acquired at several magnifications. The chemical analysis of microbeads was carried out using attenuated total reflectance-Fourier transform infrared spectroscopy (ATR-FTIR) by Spectrum One spectrometer (Perkin Elmer). The material under investigation was directly laid upon the ATR crystal, and the spectra were recorded in the wave number range of 4000–550 cm^{-1}.

2.4. Near-infrared radiation and release rate of the microbeads

Microbeads were transferred on a 96-well plate (Corning) with 100 µL of culture medium. The plate was placed under an 808 nm laser (Laser Ever) equipped with a thermal imaging camera (Optris). Different power densities were adjusted for all the tested concentrations of GO to induce the same thermal effect, increasing from room temperature to 39°C: 0.91, 2.40, and 3.30 W/cm^2 for bioinks having 0.5, 0.2, and 0.1 mg/mL of GO, respectively. Thermal increase was recorded in a time span of 60 s. To measure the release rate of the secretome, fluorescein-5-isothiocyanate (FITC)–Dextran macromolecules having a molecular weight of 10,000 kDa were embedded in the bioink. After irradiation, fluorescence of the supernatant was observed by removing the microbeads at different timepoints. Fluorescence intensity of the supernatant of non-irradiated beads was subtracted for each sample, to consider the natural swelling of the bioprinted beads. Cumulative release was then plotted over time.

2.5. Cell viability and production of reactive oxygen species

Cells were first treated with hydrogen peroxide (H_2O_2) at 250 µM for 30 min or with 1× PBS (control group). After incubation, to measure viability, cells were put in contact with bioprinted microbeads having concentrations of GO ranging from 0.5 to 0.1 mg/mL. After NIR irradiation, cells were incubated for 72 h at 37°C and 5% CO_2. Then, viability was measured using CellTiter-Glo® (Promega). Briefly, an amount of CellTiter-Glo® reagent equal to the volume of culture medium was added to each well. Then, the plate was orbitally shaken for 2 m to ensure complete cell lysis and incubated in the dark at room temperature for 10 min. After incubation, luminescence was recorded using Cytation 3 cell imaging multi-mode reader. Results were reported as % of control (untreated) cells. To observe viable cells through fluorescence microscopy, cells were stained with calcein AM (Invitrogen). Culture medium was removed, and calcein at a final concentration of 10 µM in PBS was added for 20 min at 37°C and 5% CO_2. Then, calcein was removed and replaced with culture medium. Fluorescence was observed under the fluorescence

microscope of Cytation 3. The number of viable cells was quantified using ImageJ software. For the detection of reactive oxygen species (ROS), the fluorinated derivative of 2′,7′-di-chlorofluorescein (H_2DCFDA; Sigma-Aldrich) was employed. This probe is non-fluorescent until the acetate groups are removed by intracellular esterases and oxidation occurs within cells. Thus, oxidation can be detected by monitoring the increase in fluorescence intensity. Cells were first treated with H_2O_2 at 250 μM for 30 min or with 1× PBS (control group). Microbeads were then irradiated with an 808 nm laser for 1 min. After a recovery time of 30 min, the medium was carefully washed and replaced with 1× PBS containing 10 μM H_2DCFDA. Cells were incubated for an additional hour at 37°C and 5% CO_2. PBS containing H_2DCFDA was then removed, and spheroids were resuspended in complete medium. Fluorescence intensity of H_2DCFDA was recorded by using a Cytation 3 by exciting at 495 nm and recording emission at 528 nm. Results were expressed as % of control (untreated) cells.

2.6. Statistical analysis

All measurements were performed in triplicate, and data are reported as mean ± standard deviation. Statistical analysis was performed using one-way analysis of variance (ANOVA), followed by Tukey's *post-hoc* test. Differences were considered significant when $p < 0.05$.

3. Results and discussion

3.1. Characterization of alginate-graphene oxide microbeads

In this study, we aimed to stimulate regeneration of neural cells through the controlled release of the secretome of MSCs using bioprinted AGO microbeads. To achieve this goal, we first bioprinted AGO microbeads with a homogeneous size distribution, with a peak at 200 μm (Figure 1A and B). To explore the surface structure of AGO microbeads, we acquired SEM images at different magnifications: 3000× and 10,000× (Figure 1C, top and bottom, respectively). We highlighted alginate polymers having a fiber-like shape all over the surface of the sample (green square), along with GO sheets having different lateral size, as expected (red square). Different concentrations of GO, ranging from 0.1 to 0.5 mg/mL, were used to observe any potential differences in biocompatibility and the release of MSC secretome. Neural cells were then incubated with AGO microbeads for 24 h, and viability was evaluated as a percentage of control (untreated) cells (Figure 1D). We found that even the highest tested concentration of GO did not cause any significant loss in viability, indicating the great biocompatibility of AGO microbeads. To evaluate the surface chemical composition of AGO microbeads, we performed FTIR analysis (Figure 1E). We depicted the typical O-H stretching peak of GO in the broad band from 3600 to 2400 cm^{-1}[55]. We also observed two peaks in the fingerprint region, at 1600 and 1422 cm^{-1}, which are present both in GO and, particularly, in alginate[56]. The presence of different absorption peaks in the spectroscopy of Figure 1F confirmed the successful loading of AGO microbeads with secretome. We then investigated the thermal responsiveness of bioprinted AGO microbeads by setting our experiment to reach a mild increase in temperature, up to 39°C from room temperature (Figure 1G). We used different power densities of the infrared laser to achieve the same thermal increase after NIR irradiation. To evaluate the cumulative release of the MSCs secretome over time, we embedded a fluorescent probe, FITC–Dextran, into the bioprinted AGO microbeads. We irradiated the microbeads and monitored the rate of increase in fluorescence over time (Figure 1H). We observed that the release of MSC secretome from AGO microbeads was dependent on the concentration of GO. Interestingly, the highest cumulative release was achieved with AGO microbeads having a GO concentration of 0.5 mg/mL. Taken together, our results suggest that AGO microbeads have great biocompatibility and can be used for various biological applications. Additionally, the release of molecules from AGO microbeads can be finely controlled using NIR irradiation. This characteristic makes AGO microbeads an excellent candidate for controlled drug delivery applications, where precise dosing is critical.

3.2. Biological effect of near-infrared irradiation of microbeads on damaged neural cells

We conducted an evaluation on the impact of NIR irradiation on damaged neural cells to assess the potential of AGO microbeads in stimulating cell proliferation and reducing the production of ROS. To accomplish this, we initially subjected neural cells to H_2O_2 incubation at a concentration of 250 μM. Subsequently, we introduced AGO microbeads to the cells and administered NIR irradiation at previously characterized power densities. The outcomes of our investigation are presented in Figure 2. Upon NIR irradiation, the neural cells exhibited sustained high cell viability compared to control cells (Figure 2B). Nevertheless, following the induction of toxicity through H_2O_2, no notable increase in cell viability was observed across all tested concentrations of GO, demonstrating similar outcomes to the treatment with H_2O_2 alone (Figure 2C). Notably, a slight enhancement in cell viability was observed at a GO concentration of 0.5 mg/mL. The application of NIR irradiation at all tested GO concentrations resulted in ROS levels within physiological ranges (Figure 2D). Conversely, after H_2O_2 treatment, ROS levels significantly increased for all samples (Figure 2E). Interestingly, AGO at a concentration of 0.5 mg/mL exhibited a strong reduction in ROS

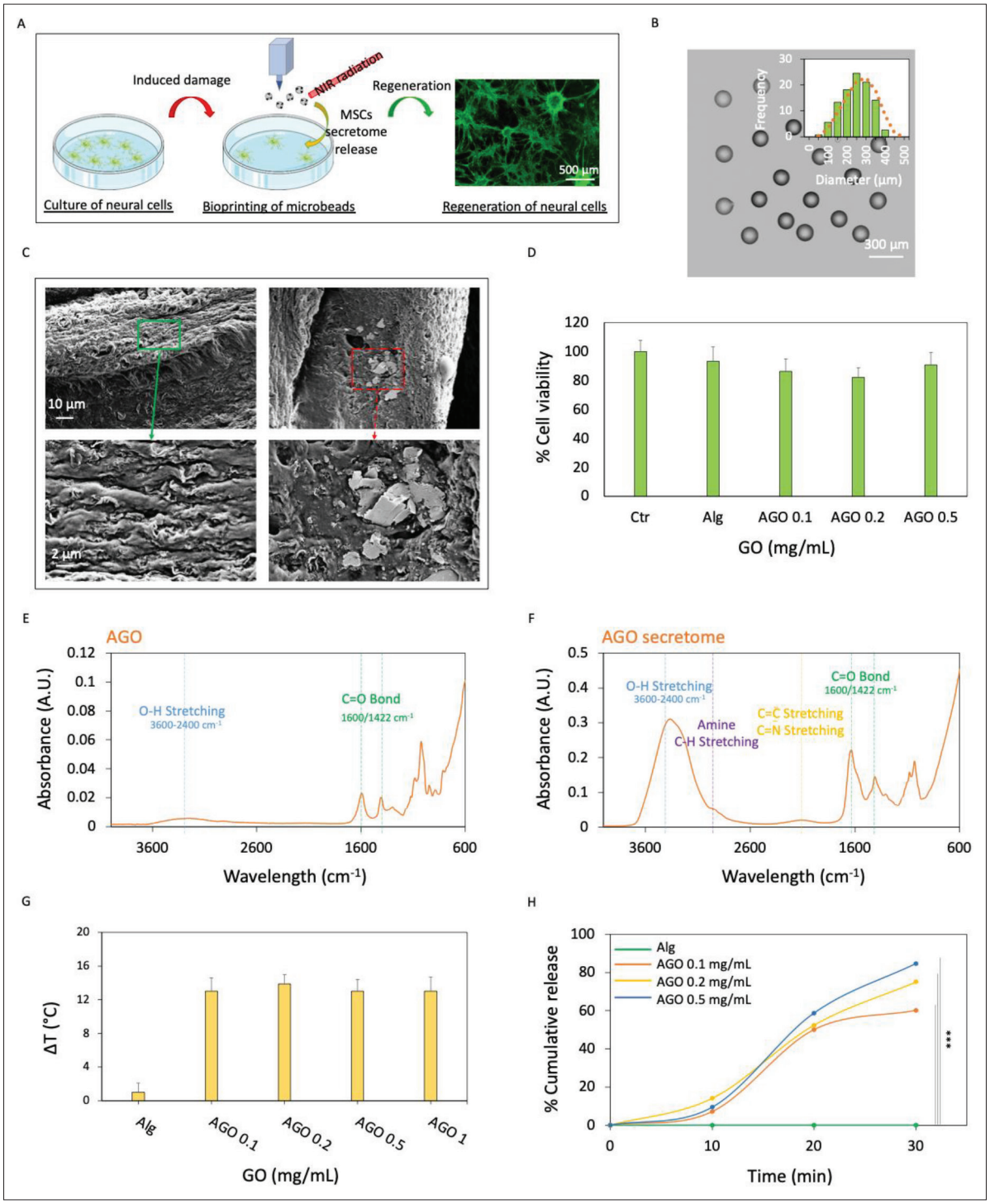

Figure 1. Bioprinting and characterization of alginate-graphene oxide microbeads. (A) Schematic illustration of the experimental setup, from bioprinting of microbeads to NIR. (B) Bright-field image of the microbeads. (C) SEM images at different magnifications of microbeads, highlighting alginate polymers (green) and GO sheets (red). (D) Biocompatibility of microbeads having different concentrations of GO. (E) FTIR analysis of microbeads, showing typical peaks of alginate and GO. (F) FTIR analysis of microbeads loaded with the secretome of mesenchymal stem cells. (G) Thermal responsiveness of the microbeads with different concentrations of GO. (H) Cumulative release over time of FITC–Dextran from microbeads after infrared radiation. ***$p < 0.01$, one-way ANOVA and Tukey's *post-hoc* test.

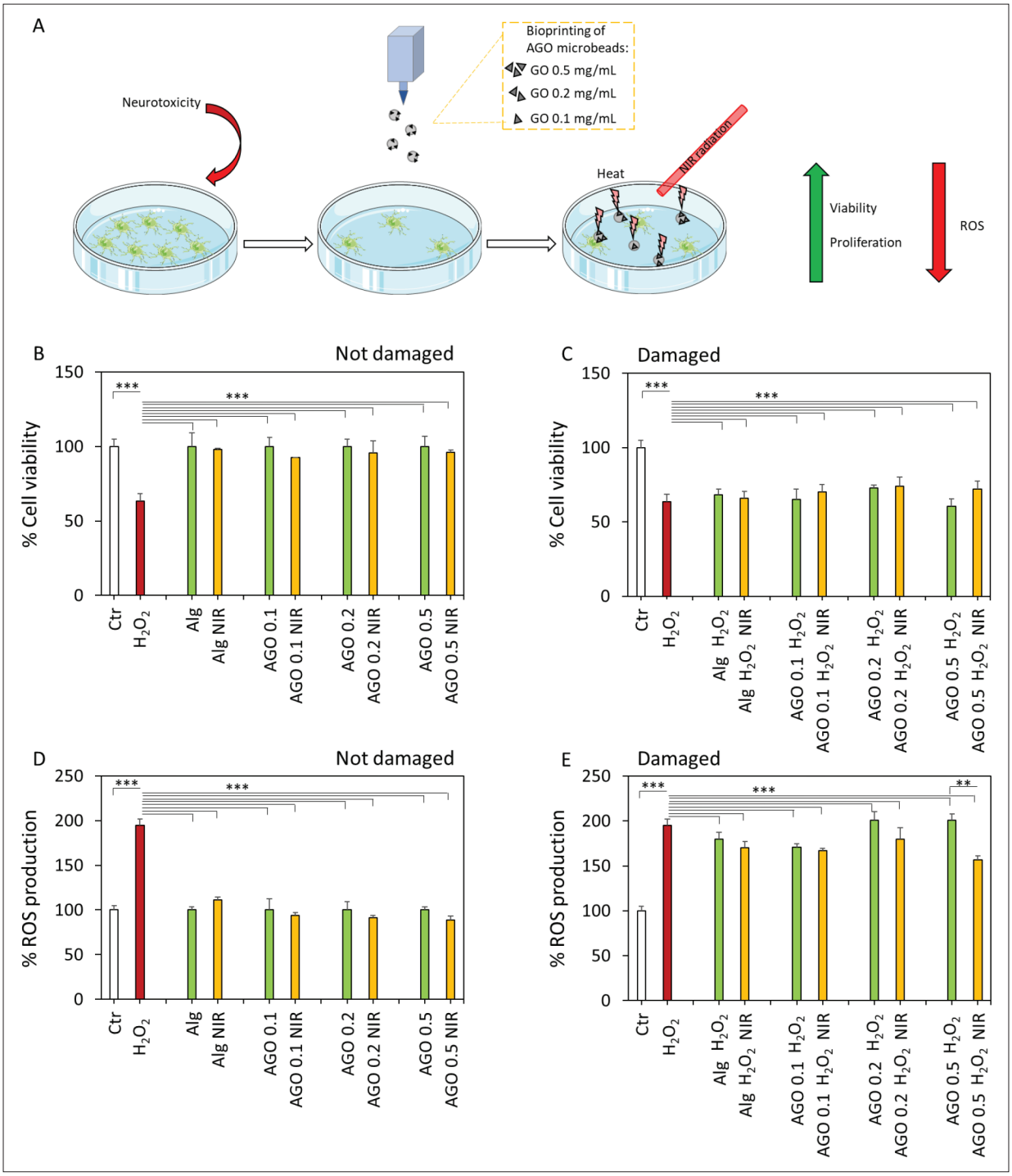

Figure 2. Biological effect of near-infrared radiation on neural cells after induced damage. (A) Schematic representation of the experimental setup. (B, C) Cell viability without or with the induction of damage with H_2O_2. (D, E) ROS production without or with the induction of damage with H_2O_2. Results are reported as % mean ± standard deviation. $^{**}p < 0.05$ and $^{***}p < 0.01$, one-way ANOVA and Tukey's *post-hoc* test.

production compared to both the H_2O_2 treatment and the positive control ($p < 0.05$, one-way ANOVA and Tukey's *post-hoc* test). The other GO concentrations did not appear to affect ROS levels.

Additionally, cell imaging through calcein staining following induced damage and NIR irradiation further emphasized a slight increase in cell number after NIR irradiation of AGO at a concentration of 0.5 mg/mL, in line

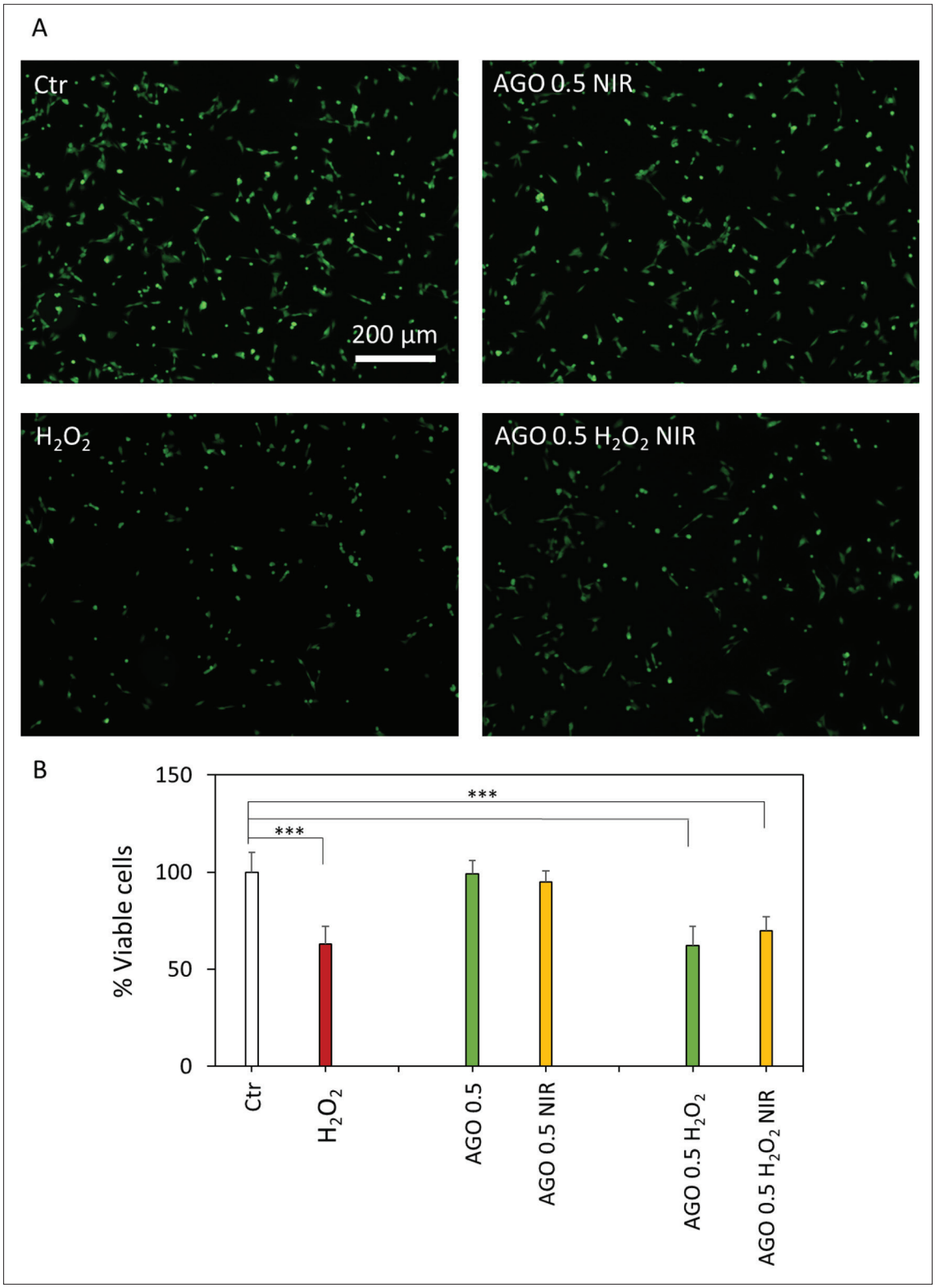

Figure 3. Staining of viable cells with calcein AM. (A) Representative images with calcein AM staining of cells and relative quantification of the number of viable cells after near-infrared radiation of alginate microbeads having graphene oxide at 0.5 mg/mL. (B) Quantification of viable cells based on calcein images. Results are reported as % of control cells. ***$p < 0.01$, one-way ANOVA and Tukey's *post-hoc* test.

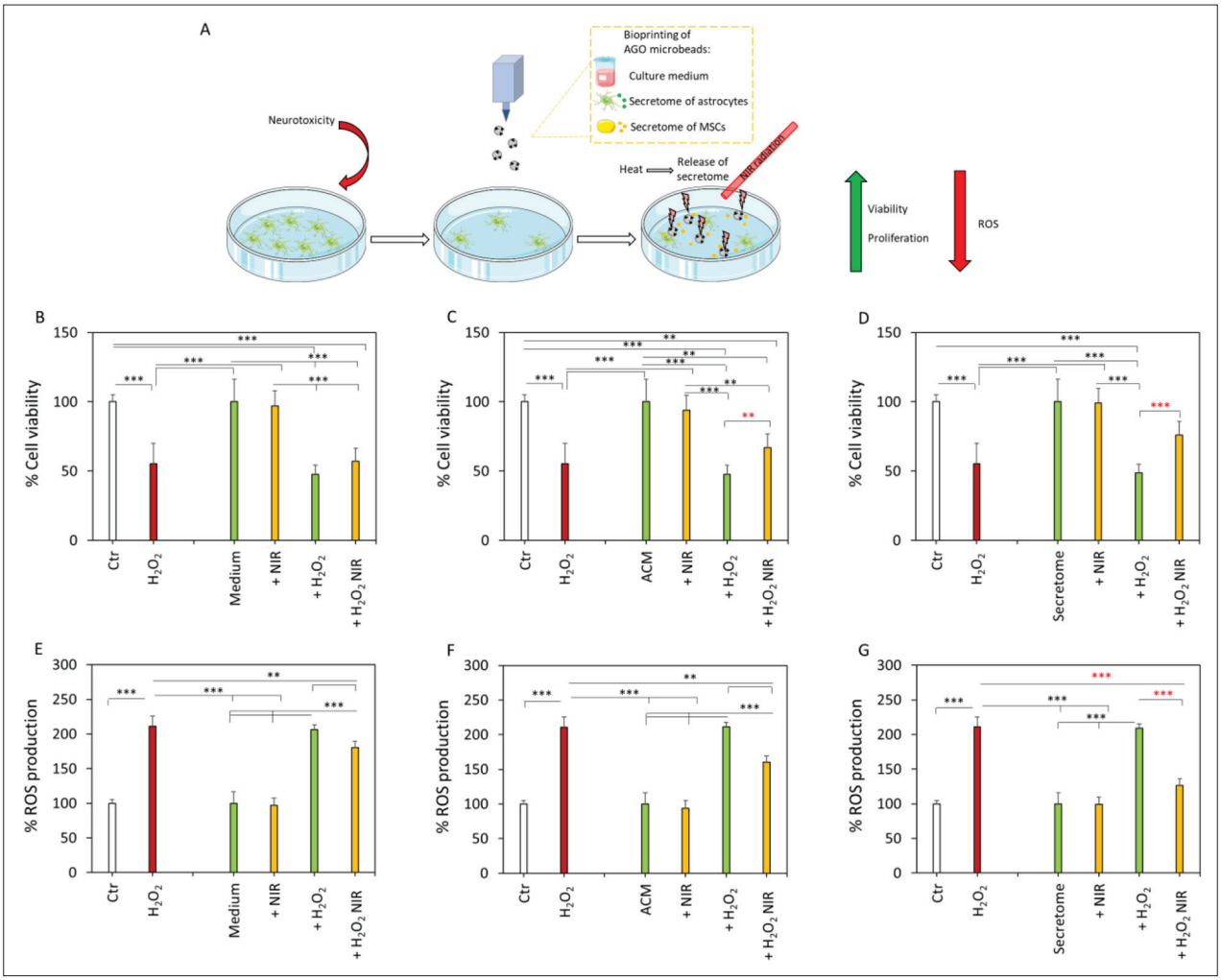

Figure 4. Biological effect on neural cells of the release of secretome through near-infrared radiation after induced damage. (A) Schematic representation of the experimental setup. (B–D) Cell viability after the induction of damage with H_2O_2 and controlled release of culture medium, astrocyte-conditioned medium, and secretome of mesenchymal stem cells, respectively. (E–G) ROS production after the induction of damage with H_2O_2 and controlled release of culture medium, astrocyte-conditioned medium, and secretome of mesenchymal stem cells, respectively. Results are reported as % mean ± standard deviation. $^{**}p < 0.05$ and $^{***}p < 0.01$, one-way ANOVA and Tukey's *post-hoc* test.

with the cell viability data (Figure 3A and B). Our findings indicate that for evaluating the effectiveness and potential of MSCs secretome in regenerating neural cells, bioprinted AGO microbeads at a GO concentration of 0.5 mg/mL offer the most suitable configuration due to their elevated release of FITC–Dextran and their ability to downregulate ROS levels. As a result, we selected this GO concentration for our subsequent experiments.

3.3. Biological effect of the secretome of mesenchymal stem cells through near-infrared controlled release on damaged neural cells

We then bioprinted AGO microbeads having GO at 0.5 mg/mL, in which we embedded the secretome of MSCs. It has widely been reported in the literature that not only the secretome, but also the set of factors and vesicles released by astrocytes (namely astrocyte-conditioned medium, ACM) displays a strong potential for the regeneration and proliferation of neural cells. For this purpose, we bioprinted AGO microbeads having embedded ACM to compare their effectiveness with the secretome of MSCs and with standard culture medium as a negative control. Results are reported in Figure 4. After NIR irradiation, the release of culture medium caused a mild increase in cell viability, similar to the previous finding (Figure 4B). The release of ACM, importantly, caused a strong increase in cell viability, which resulted to be 67% ± 11.1% with respect to cells having induced neural damage with H_2O_2, which resulted to be 47% ± 9.3% (Figure 4C, $p < 0.05$, one-way ANOVA and Tukey's *post-hoc* test). After controlled release

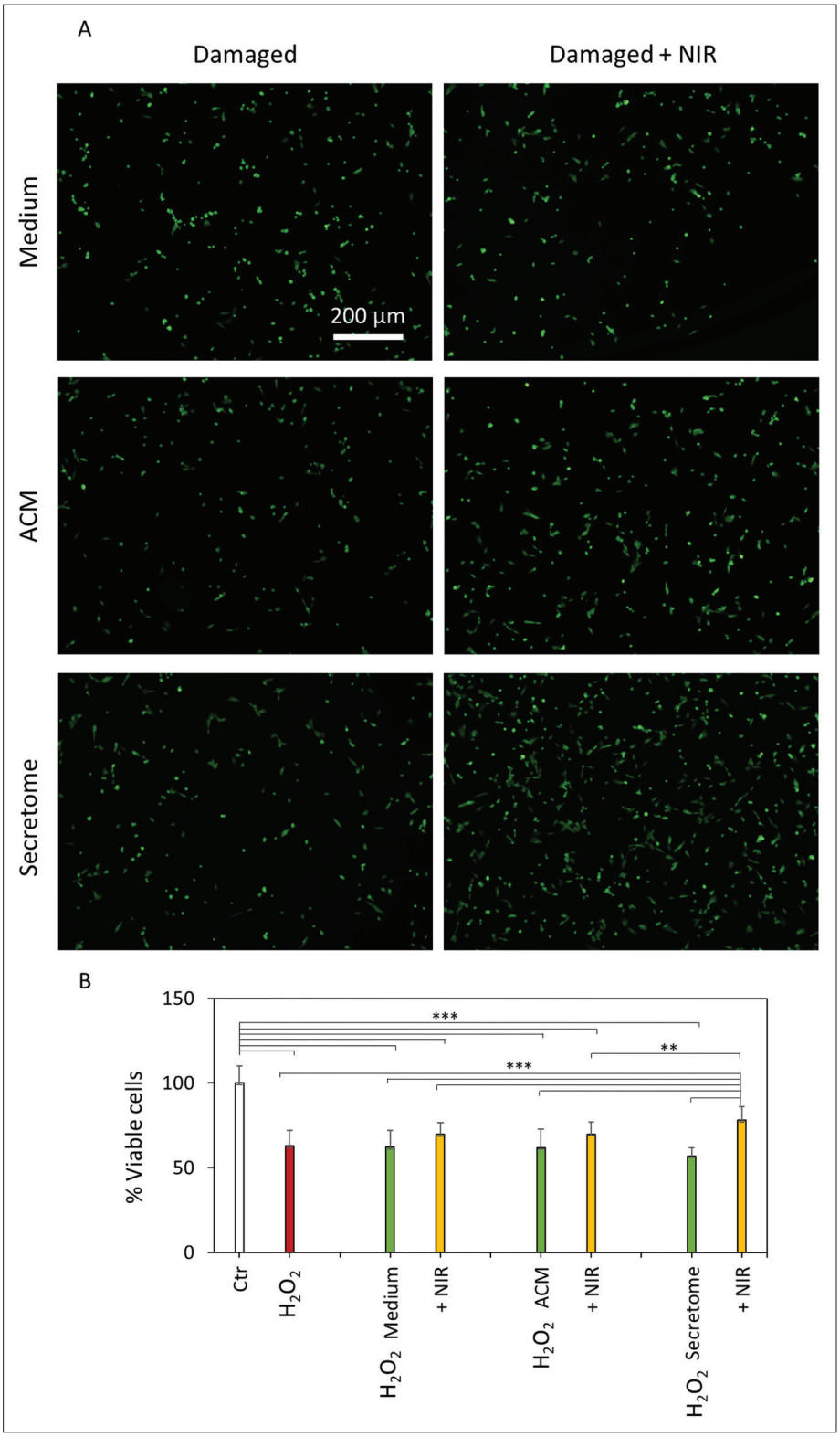

Figure 5. Staining of viable cells with calcein AM. (A) Representative images with calcein AM staining of damaged cells after controlled release of the culture medium, astrocyte-conditioned medium, and secretome. (B) Quantification of viable cells based on calcein images. Results are reported as % of control cells. $^{**}p < 0.05$ and $^{***}p < 0.01$, one-way ANOVA and Tukey's *post-hoc* test.

of MSCs secretome, importantly, a significantly strong recover of cell viability was observed in neural cells, which reached 76% ± 1.8% (Figure 4D, $p < 0.05$, one-way ANOVA and Tukey's *post-hoc* test). The production of ROS was also monitored after neural damage and NIR irradiation. The release of culture medium mildly affected the production of free radicals, reducing the levels from 206% ± 28.4% of the positive control down to 180% ± 23.6% (Figure 4E, $p < 0.05$, one-way ANOVA and Tukey's *post-hoc* test). The release of ACM after NIR had an even stronger effect on ROS of neural cells, reducing their production to 160% ± 29.5% (Figure 4F, $p < 0.05$, one-way ANOVA and Tukey's *post-hoc* test). Finally, the release of MSCs secretome had the strongest effect even on the production of ROS, which was significantly reduced to 126% ± 3.4% (Figure 4G, $p < 0.01$, one-way ANOVA and Tukey's *post-hoc* test).

Calcein staining furtherly confirmed viability and ROS production data, indicating a significantly higher cell proliferation in neural cells after recovery with MSCs secretome with respect to the other treatments (Figure 5A and B). Our findings demonstrate that the secretome of MSCs holds immense regenerative potential for nerve repair. Its controlled release from AGO microbeads showcases superior efficacy in enhancing cell viability and reducing ROS production in damaged neural cells, surpassing the effects observed with ACM and standard culture medium. These findings offer promising insights into the therapeutic applications of MSC secretome in nerve regeneration, highlighting its significance in future research and clinical interventions.

4. Conclusion

Our study presents a novel approach for the controlled delivery of MSCs secretome for neuronal regeneration using NIR-responsive bioprinted AGO microbeads. By encapsulating the MSCs' secretome in AGO microbeads and utilizing NIR radiation, we successfully achieved the controlled release of therapeutic factors for promoting neuronal proliferation, survival, and viability. Our findings highlight the efficacy of the MSCs secretome in promoting neural proliferation compared to the secretome derived from astrocytes, a known promoter of nerve regeneration. The controlled release of the MSCs secretome through non-invasive NIR radiation from AGO microbeads demonstrated significant benefits in terms of neuronal proliferation and regeneration following induced toxicity. This approach offers advantages over conventional delivery methods, such as precise control over the timing, location, and dosage of therapeutic agents. The use of AGO microbeads not only allows for controlled release but also provides additional benefits, including potential reductions in immunogenicity and tumorigenicity. Furthermore, due to the easy and repeatable production of alginate and GO, along with the easy storage and stability, future large-scale production of these AGO particles will be achievable. These advantages make AGO microbeads a promising platform for the development of MSC-based therapies for neuronal recovery after injury. This innovative approach holds great potential for the treatment of various neuropathies and injuries, offering new possibilities for enhancing patient outcomes and quality of life. Further research is warranted to explore the underlying mechanisms of action and optimize the parameters of NIR-responsive delivery systems. Future studies regarding the biodistribution of microbeads after local injection will have to be performed. The development of robust and safe MSC-based therapies utilizing the controlled delivery of the secretome holds promise for addressing the unmet clinical needs in neuronal regeneration and providing effective treatments for patients with neurological disorders and injuries.

Acknowledgments

None.

Funding

Not applicable.

Conflict of interest

The authors declare no conflict of interest.

Author contributions

Conceptualization: Massimiliano Papi, Marco De Spirito
Formal analysis: Giordano Perini
Investigation: Giordano Perini, Valentina Palmieri, Marcello D'Ascenzo, Claudia Colussi
Methodology: Ginevra Friggeri, Alberto Augello, Lishan Cui
Writing – original draft: Giordano Perini
Writing – review & editing: Massimiliano Papi, Claudio Grassi, Marco De Spirito

Ethics approval and consent to participate

Animal procedures (E18 isolation and neuronal cultures) were approved by the Ethical Committee of the Università Cattolica del Sacro Cuore (authorization n° 494/2022-PR) and were fully compliant with Italian (Ministry of Health guidelines, Legislative Decree No. 116/1992) and European Union (Directive No. 86/609/EEC) legislations on animal research.

Consent for publication

Not applicable.

Availability of data

The data that support the findings of this study are available from the corresponding author upon reasonable request.

References

1. Aktas O, Ullrich O, Infante-Duarte C, *et al.*, 2007, Neuronal damage in brain inflammation. *Arch Neurol,* 64(2): 185–189.
2. Tarkowski E, Liljeroth A-M, Minthon L, *et al.,* 2003, Cerebral pattern of pro- and anti-inflammatory cytokines in dementias. *Brain Res Bull,* 61(3): 255–260.
3. White MG, Luca LE, Nonner D, *et al.,* 2007, Cellular mechanisms of neuronal damage from hyperthermia, in *Neurobiology of Hyperthermia* (ed. Sharma HSBT-P). Neurobiology of Hyperthermia [Internet]. Elsevier, *Prog Brain Res,* 347–371. doi: 10.1016/S0079-6123(06)62017-7. PMID: 17645927.
4. Everall I, Luthert P, Lantos P, 1993, A review of neuronal damage in human immunodeficiency virus infection: Its assessment, possible mechanism and relationship to dementia. *J Neuropathol Exp Neurol,* 52(6): 561–566.

   https://doi.org/10.1097/00005072-199311000-00002
5. Guo J, Zhao X, Li Y, *et al.*, 2018, Damage to dopaminergic neurons by oxidative stress in Parkinson's disease. *Int J Mol Med,* 41(4): 1817–1825.
6. Blandini F, 2013, Neural and immune mechanisms in the pathogenesis of Parkinson's disease. *J Neuroimmune Pharmacol,* 8(1): 189–201.

   https://doi.org/10.1007/s11481-013-9435-y
7. Perini G, Ciasca G, Minelli E, *et al.,* 2019, Dynamic structural determinants underlie the neurotoxicity of the N-terminal tau 26-44 peptide in Alzheimer's disease and other human tauopathies. *Int J Biol Macromol,* 141: 278–289.
8. Zhang M, Cheng X, Dang R, *et al.,* 2018, Lactate deficit in an Alzheimer disease mouse model: The relationship with neuronal damage. *J Neuropathol Exp Neurol,* 77(12): 1163–1176.

   https://doi.org/10.1093/jnen/nly102
9. Patejdl R, Zettl UK, 2017, Spasticity in multiple sclerosis: Contribution of inflammation, autoimmune mediated neuronal damage and therapeutic interventions. *Autoimmun Rev,* 16(9): 925–936.
10. Malgouris C, Bardot F, Daniel M, *et al.,* 1989, Riluzole, a novel antiglutamate, prevents memory loss and hippocampal neuronal damage in ischemic gerbils. *J Neurosci,* 9(11): 3720–3727.
11. Languren G, Montiel T, Julio-Amilpas A, *et al.,* 2013, Neuronal damage and cognitive impairment associated with hypoglycemia: An integrated view. *Neurochem Int,* 63(4): 331–343.
12. Corrigan JD, Selassie AW, Orman JAL, 2010, The epidemiology of traumatic brain injury. *J Head Trauma Rehabil,* 25(2): 72–80.
13. Sapolsky RM, Krey LC, McEwen BS, 1985, Prolonged glucocorticoid exposure reduces hippocampal neuron number: Implications for aging. *J Neurosci,* 5(5): 1222–1227.
14. Biffi A, Capotondo A, Fasano S, *et al.,* Gene therapy of metachromatic leukodystrophy reverses neurological damage and deficits in mice. *J Clin Invest,* 116(11): 3070–3082.
15. Amar AP, Levy ML, 1999, Pathogenesis and pharmacological strategies for mitigating secondary damage in acute spinal cord injury. *Neurosurgery,* 44(5): 1027–1039.
16. Dutta R, Trapp BD, 2007, Pathogenesis of axonal and neuronal damage in multiple sclerosis. *Neurology,* 68(22 suppl 3): S22–S31.
17. Baron R, 2000, Peripheral neuropathic pain: From mechanisms to symptoms. *Clin J Pain,* 16(2): S12–S20.
18. Rosenthal P, Borsook D, Moulton EA, 2016, Oculofacial pain: Corneal nerve damage leading to pain beyond the eye. *Invest Ophthalmol Vis Sci,* 57(13): 5285–5287.
19. Kurnellas MP, Donahue KC, Elkabes S, 2007, Mechanisms of neuronal damage in multiple sclerosis and its animal models: Role of calcium pumps and exchangers. *Biochem Soc Trans,* 35(5): 923–926.
20. Zipp F, Gold R, Wiendl H, 2013, Identification of inflammatory neuronal injury and prevention of neuronal damage in multiple sclerosis: Hope for novel therapies? *JAMA Neurol,* 70(12): 1569–1574.
21. Meeson R, Corr S, 2011, Management of pelvic trauma: Neurological damage, urinary tract disruption and pelvic fractures. *J Feline Med Surg,* 13(5): 347–361.
22. Crock HV, Crock HV, 1983, The management of spinal injuries with and without neural damage. *Pract Spinal Surg,* 281–298.
23. Bechstein WO, 2000, Neurotoxicity of calcineurin inhibitors: Impact and clinical management. *Transpl Int,* 13(5): 313–326.
24. Yamakami I, Yamaura A, Isobe K, 1993, Pathogenesis and management of secondary neural damage in head trauma patients: Analysis of patients who talk and deteriorate" fulminantly". *No Shinkei Geka,* 21(2): 129–133.
25. Bejargafshe MJ, Hedayati M, Zahabiasli S, *et al.,* 2019, Safety and efficacy of stem cell therapy for treatment of neural damage in patients with multiple sclerosis. *Stem Cell Investig,* 6: 44.
26. Wong AM, Hodges H, Horsburgh K, 2005, Neural stem cell grafts reduce the extent of neuronal damage in a mouse model of global ischaemia. *Brain Res,* 1063(2): 140–150.
27. Karl MO, 2013, The potential of stem cell research for the treatment of neuronal damage in glaucoma. *Cell Tissue Res,* 353(2): 311–325.

28. Qin J, *et al.,* 2015, Transplantation of induced pluripotent stem cells alleviates cerebral inflammation and neural damage in hemorrhagic stroke. *PLoS One,* 10(6): e0129881.

29. Ma X, *et al.,* 2020, ADSCs-derived extracellular vesicles alleviate neuronal damage, promote neurogenesis and rescue memory loss in mice with Alzheimer's disease. *J Control Release,* 327: 688–702.

30. Bora P, Majumdar AS, 2017, Adipose tissue-derived stromal vascular fraction in regenerative medicine: A brief review on biology and translation. *Stem Cell Res Ther,* 8(1): 145.

    https://doi.org/10.1186/s13287-017-0598-y

31. Teixeira FG, Carvalho MM, Sousa N, *et al*., 2013, Mesenchymal stem cells secretome: A new paradigm for central nervous system regeneration? *Cell Mol Life Sci,* 70: 3871–3882.

32. Drago D, Cossetti C, Iraci N, *et al.,* 2013, The stem cell secretome and its role in brain repair. *Biochimie,* 95(12): 2271–2285.

33. Ghasemi M, Roshandel E, Mohammadian M, *et al.,* Mesenchymal stromal cell-derived secretome-based therapy for neurodegenerative diseases: Overview of clinical trials. *Stem Cell Res Ther,* 14(1): 1–20.

34. Carvalho M, Teixeira F, Reis R, *et al.*, 2011, Mesenchymal stem cells in the umbilical cord: phenotypic characterization, secretome and applications in central nervous system regenerative medicine. *Curr Stem Cell Res Ther,* 6(3): 221–228.

35. Martins LF, Costa RO, Pedro JR, *et al.,* 2017, Mesenchymal stem cells secretome-induced axonal outgrowth is mediated by BDNF. *Sci Rep,* 7(1): 4153.

36. Teixeira FG, Salgado AJ, 2020, Mesenchymal stem cells secretome: Current trends and future challenges. *Neural Regen Res,* 15(1): 75.

37. Kumar P, Kandoi S, Misra R, *et al.,* 2019, The mesenchymal stem cell secretome: A new paradigm towards cell-free therapeutic mode in regenerative medicine. *Cytokine Growth Factor Rev,* 46: 1–9.

38. Li F, Zhang J, Yi K, Wang H, *et al.,* 2022, Delivery of stem cell secretome for therapeutic applications. *ACS Appl Bio Mater,* 5(5): 2009–2030.

39. Wechsler ME, Rao VV, Borelli AN, *et al.*, 2021, Engineering the MSC secretome: A hydrogel focused approach. *Adv Healthc Mater,* 10(7): 2001948.

40. Santamaria G, Brandi E, Vitola P La, *et al.,* 2021, Intranasal delivery of mesenchymal stem cell secretome repairs the brain of Alzheimer's mice. *Cell Death Differ,* 28(1): 203–218.

41. Shoma Suresh K, Bhat S, Guru BR, *et al.*, 2020, A nanocomposite hydrogel delivery system for mesenchymal stromal cell secretome. *Stem Cell Res Ther,* 11(1): 1–14.

42. Perini G, Rosenkranz A, Friggeri G, *et al.,* 2022, Advanced usage of Ti3C2Tx MXenes for photothermal therapy on different 3D breast cancer models. *Biomed Pharmacother,* 153: 113496.

43. Rosenkranz A, Perini G, Aguilar-Hurtado JY, *et al.,* 2021, Laser-mediated antibacterial effects of few- and multi-layer Ti3C2Tx MXenes. *Appl Surf Sci,* 567: 150795.

44. Perini G, Rosa E, Friggeri G, *et al.,* 2022, INSIDIA 2.0 high-throughput analysis of 3D cancer models: Multiparametric quantification of graphene quantum dots photothermal therapy for glioblastoma and pancreatic cancer. *Int J Mol Sci,* 23: 3217.

45. Perini G, Palmieri V, Friggeri G, *et al.,* 2023, Carboxylated graphene quantum dots-mediated photothermal therapy enhances drug-membrane permeability, ROS production, and the immune system recruitment on 3D glioblastoma models. *Cancer Nanotechnol,* 14(1): 13.

46. De Maio F, Rosa E, Perini G, *et al.,* 2022, 3D-printed graphene polylactic acid devices resistant to SARS-CoV-2: Sunlight-mediated sterilization of additive manufactured objects. *Carbon NY,* 194: 34–41.

47. Choi SS, Lee HJ, Lim I, *et al.*, 2014, Human astrocytes: Secretome profiles of cytokines and chemokines. *PLoS One,* 9(4): e92325.

48. Skorupa A, Urbach S, Vigy O, *et al.,* 2013, Angiogenin induces modifications in the astrocyte secretome: Relevance to amyotrophic lateral sclerosis. *J Proteomics,* 91: 274–285.

49. Jha MK, Seo M, Kim J-H, *et al.,* 2013, The secretome signature of reactive glial cells and its pathological implications. *Biochim Biophys Acta (BBA)-Proteins Proteomics,* 1834(11): 2418–2428.

50. Tanaka J, Toku K, Zhang B, *et al.,* 1999, Astrocytes prevent neuronal death induced by reactive oxygen and nitrogen species. *Glia,* 28(2): 85–96.

51. Madrigal JLM, Leza JC, Polak P, *et al.*, 2009, Astrocyte-derived MCP-1 mediates neuroprotective effects of noradrenaline. *J Neurosci,* 29(1): 263–267.

52. Pei X, Li Y, Zhu L, *et al.*, 2019, Astrocyte-derived exosomes suppress autophagy and ameliorate neuronal damage in experimental ischemic stroke. *Exp Cell Res,* 382(2): 111474.

53. Piacentini R, Li Puma DD, Ripoli C, *et al.,* 2015, Herpes Simplex Virus type-1 infection induces synaptic dysfunction in cultured cortical neurons via GSK-3 activation and intraneuronal amyloid-β protein accumulation. *Sci Rep,* 5(1): 15444.

54. Perini G, Palmieri V, Ciasca G, *et al.,* 2020, Graphene quantum dots' surface chemistry modulates the sensitivity of glioblastoma cells to chemotherapeutics. *Int J Mol Sci,* 21(17): 6301.

55. Guo S, Garaj S, Bianco A, *et al.*, 2022, Controlling covalent chemistry on graphene oxide. *Nat Rev Phys,* 4(4): 247–262.

56. Mollah MZI, Faruque MRI, Bradley DA, *et al.*, 2023, FTIR and rheology study of alginate samples: Effect of radiation. *Radiat Phys Chem,* 202: 110500.